Intrinsic Modulation of Pulse–Coupled Integrate–and–Fire Neurons

S. Coombes

Nonlinear and Complex Systems Group, Department of Mathematical Sciences, Loughborough University, Leicestershire, LE11 3TU, UK.

G. J. Lord

Applied Nonlinear Mathematics Group, Department of Engineering Mathematics, Bristol University, University Walk, Bristol, BS8 1TR, UK.

(May 2, 1997)

Abstract

Intrinsic neuromodulation is observed in sensory and neuromuscular circuits and in biological central pattern generators. We model a simple neuronal circuit with a system of two pulse–coupled integrate–and–fire neurons and explore the parameter regimes for periodic firing behaviour. The inclusion of biologically realistic features shows that the speed and onset of neuronal response plays a crucial role in determining the firing phase for periodic rhythms. We explore the neurophysiological function of distributed delays arising from both the synaptic transmission process and dendritic structure as well as discrete delays associated with axonal communication delays. Bifurcation and stability diagrams are constructed with a mixture of simple analysis, numerical continuation and the Kuramoto phase–reduction technique. Moreover, we show how realistic forms of voltage dependent shunting synaptic currents can act to limit the firing rate of the system, and that, for asynchronous

behaviour, the strength of electrical synapses can control such rates.

87.10+e,0.2.30.Ks, 47.20.Ky

I. INTRODUCTION

There are two sources of modulation for neuronal circuits: extrinsic, such as an external input, and intrinsic, such as variation of cell membrane properties. Intrinsic modulation is thought to produce local changes in neuronal computation in contrast to extrinsic modulation that can cause global changes [1]. This is well illustrated with the example of the neuronal circuits found in the crustacean stomatogastric ganglion [2]. Altering cellular and synaptic properties of neurons in this circuit causes different dynamical network behaviour and hence to the generation of distinct gastric rhythms [3]. Circuits which, by virtue of their intrinsic properties and synaptic interactions, generate and control the activity of motor neurons are called central pattern generators (CPGs). Intrinsic neuromodulation has been experimentally demonstrated in several biological CPGs [1,4,5], where a diverse repertoire of rhythmic motor behaviour is possible in the absence of sensory feedback. It is believed that a brief initial stimulus triggers the intrinsic neuromodulation that arises from neurons within the CPG circuit allowing the production of a prolonged rhythmic pattern. For example, in the mollusc Tritonia [1] and the tadpole Xenopus [4] the escape swim behaviour is generated in this fashion.

The study of coupled oscillators has applications in understanding CPG neuronal circuits such as those mentioned above. Indeed, systems of coupled nonlinear oscillators have recently attracted much interest in neurobiology due to the discovery of synchronised oscillations in the cat visual cortex [6]. Much of the theoretical work in this area uses the phase–coupled oscillator formalism developed by Kuramoto [7]. Moreover, there is also considerable interest in studying the dynamics of pulse–coupled neuronal models in which the details of individual spikes are included (see [8] for a review). The analysis of reciprocally connected neurons has implications for understanding the mechanisms whereby rhythm generation (periodic behaviour) is produced by a CPG in the absence of endogenous pacemaking cells. Reduced versions of the Hodgkin–Huxley equations including details of ionic currents have been studied numerically [9–13] whilst the analysis of coupled relaxation oscillators has

allowed a more analytic approach [14]. We are careful to distinguish three forms of oscillations: a synchronous state, where neurons oscillate in phase; anti-synchronous state, where neurons oscillate in anti-phase; and an asynchronous state, a state between the other two where neurons oscillate at an intermediate phase. In theoretical studies of pulse–coupled neuronal networks with fast synaptic responses, synchronisation is typically obtained with excitatory connections between neurons [15–17]. However, neuronal CPGs and cortical tissue can maintain synchronous, anti-synchronous and asynchronous behaviour. For example, the CPG for swimming in the tadpole Xenopus maintains an anti–phase oscillatory rhythm to generate waves of bending along the spinal cord. Inhibitory synaptic connections undoubtedly play an important role in preventing large–scale synchronisation. However, recent work suggests that other intrinsic mechanisms may also lead to desynchronisation. Van Vreeswijk *et al* [18] have shown that pulse–coupled integrate–and–fire neurons can desychronise if the post–synaptic currents are sufficiently slow. Hence, distributed delays from synaptic transmission processes can effect the synchrony of simple coupled neural oscillators. This effect is also observed when more detailed single neuron models such as Hodgkin–Huxley are studied in the limit of weak coupling with the phase reduction technique of Kuramoto [18,19]. Also, Sherman and Rinzel [20] have shown numerically that strong electrical coupling leads to synchronous behaviour for a pair of coupled neurons, but that weak electronic coupling can lead to anti–phase oscillations. Similar observations have previously been made by Mulloney *et al* [21]. A more detailed analysis of this phenomenon is undertaken by Han *et al* [22] using a combination of numerical simulation and the weak coupling phase reduction technique. They show that global electrical coupling leads to bursting behaviour as well as the previously observed desychronisation. The neuronal propagation delays present in a system of interacting neurons are also thought to provide a mechanism for desynchronisation [16]. For the case of two pulse–coupled oscillators incorporating small delays, a return–map analysis [23,24], that generalises the seminal work of Mirollo and Strogatz [15], reinforces this idea. Furthermore, in the presence of signal delays, the phase–coupled oscillator model of Kuramato possesses multiple synchronous solutions [25] for 2 neurons and exhibits extremely rich

asynchronous behaviour for a population that interacts via time–delayed nearest–neighbour coupling [26]. The Kuramoto phase reduction technique has also recently been used to analyse the effects of dendritic structure on neuronal synchronisation [27–29]. Neurons that filter synaptic input through a passive dendritic tree have responses that depend upon the distributed delays arising from the diffusion of a signal along the tree and the spatial location of the synapse.

In this paper we investigate sources of intrinsic neuromodulation for a simple model CPG. We consider a circuit of two identical integrate–and–fire neurons mutually coupled by identical excitatory synapses. The classification of dynamical behaviour in different parameter regimes can be used to model the effects of intrinsic neuromodulation provided that the model maintains contact with biological reality. We focus on features of the single neuron that affect the neuronal response to synaptic stimulation. Since these in turn contribute to the nature of a network oscillation we are able to isolate the role that various cellular and synaptic properties have in determining circuit function. Importantly, in contrast to work discussed above and extending an earlier paper [30], we show that the competition between various neuronal length and time scales has important consequences for neurophysiological function. For example, the distributed delay that arises from the synaptic transmission process may result in a slow neuronal response which in turn stabilises an asynchronous network rhythm. However, the inclusion of a further delay, arising from say a finite axonal propagation velocity, can lead to a stable synchronous rhythm. Variation of the period of oscillation, as well as the phase, is also important in many biological CPGs. Electronic parameters taking the form of cell membrane reversal potentials and electrical synapses between neurons are suggested as a possible source for the modulation of the firing period.

In detail, we take single spikes or *action potentials* as basic entities, communicated via chemical synapses. Pre–synaptic action potentials are considered to induce post–synaptic currents. These are described with functional forms that closely approximate real synaptic currents. Furthermore, we include transmission delays that model the finite axonal propagation time for action potentials. An integrate–and–fire model with linear cell membrane

properties is essentially solvable using the variation of parameters formula. In section II this approach is used to study the dynamics of the cell body (soma) of two such pulse–coupled neurons. However, real neurons typically possess voltage dependent ionic currents with specific reversal potentials. The incorporation of shunting currents into the model induces a time dependent cell membrane decay and is studied in section III. In biological CPGs with small neuronal populations, gap junctions or electrical synapses contribute significantly to network activity. The above model is extended to include bi–directional electrical synapses and re–expressed such that cell membrane potentials evolve according to a linear Volterra integro–differential equation. Once again the variation of parameters formula is used in section IV to formulate solutions. Finally, in section V, we consider the effects of dendrites on phase–synchronisation by idealising the dendritic tree as a semi–infinite one dimensional structure described by a second order linear partial differential equation, namely the cable equation [31]. Assuming that the neurons intrinsically oscillate, a completely analytic discussion of the effects of the spatial location of the synaptic input is possible using the phase reduction technique of Kuramoto [7]. Results are exact for weak synaptic coupling and the case when the somatic feedback current from the soma to the dendrites is negligible. The stability of solutions is shown to depend upon both the natural frequency of oscillation and the point of synaptic contact.

Throughout the paper detailed numerical analysis, using AUTO94 [32], is used to explore the solution spaces generated using the variation of parameters formula. In essence, motivated by biological CPGs with intrinsic neuromodulation, we explore the role that variation of propagation time–delays, rise and fall time of post synaptic current pulses, strength of chemical and electrical coupling, shunting currents, reversal potentials and dendritic structure can have on the phase of periodic firing patterns for two pulse–coupled integrate–and–fire neurons. The consequences of this work for larger arrays is discussed in section VI.

II. PULSATILE COUPLING WITH DELAYS IN AN INTEGRATE–AND–FIRE MODEL

We begin by considering two identical integrate–and–fire neurons with mutual excitatory coupling. Each neuron is regarded as a point processor with no extended dendritic structure. The state variable $\phi_i(t)$, $i = 1, 2$, is used to represent the cell membrane potential at neuron 1 and 2 respectively. The neurons are assumed to fire whenever $\phi_i(t)$ reaches some threshold h, after which $\phi_i(t)$ is reset to some resting level, taken as zero (see figure 1). Denoting the time at which neuron i fires for the nth occassion T_n^i, since the initial firing time T_0^i, the potentials $\phi_i(t)$ evolve according to the linear ordinary differential equations (ODEs)

$$\frac{\mathrm{d}\phi_i}{\mathrm{d}t} = -\frac{\phi_i}{\tau} + I_i(t) \quad t \in (T_k^i, T_{k+1}^i), \quad k \in \mathbb{Z} \tag{1}$$

with the strongly nonlinear reset conditions

$$\lim_{\epsilon \to 0_+} \phi_i(T_k^i - \epsilon) = h, \quad \lim_{\epsilon \to 0_+} \phi_i(T_k^i + \epsilon) = 0. \tag{2}$$

Here, $I_i(t)$ represents the input to neuron i from neuron j, which is therefore dependent upon the firing history of the system. Equation (1) is simply the differential equation of an RC circuit of cell membrane resistance R, capacitance C and hence, membrane time constant $\tau = RC$. Between firing events the unique solution to (1) is given using the variation of parameters formula,

$$\phi_i(t) = \int_{T_k^i}^{t} \mathrm{e}^{-(t-t')/\tau} I_i(t') \mathrm{d}t', \quad t \in (T_k^i, T_{k+1}^i). \tag{3}$$

The current $I_i(t)$ should reflect the fact that postsynaptic currents are generated by the firing events or *spikes* of the presynaptic neuron j. These spikes are often modelled as simple Dirac δ function pulses [15,17,33]. However, the effective input to the postsynaptic neuron has a longer temporal duration due to the synaptic transmission process. One particular pulse shape that approximates the rise and fall time of real synaptic currents is the so–called α–function [34]. The consequences of the temporal duration of synaptic conductance changes within integrate–and–fire models has been discussed (for the case of α–functions) by several

authors [18,35,36]. One should also be careful to incorporate delays due to finite axonal propagation times into the total synaptic current. With this in mind, we write the input to neuron i from neuron j as a sum of delayed α–functions such that,

$$I_i(t) = \sum_{n\geq 1} P(t - T_n^j - t_d)\Theta(t - T_n^j - t_d), \quad j \neq i \tag{4}$$

where t_d represents the axonal propagation delay time and $P(t)$ takes the form of an α–function:

$$P(t) = g\alpha^2 t \mathrm{e}^{-\alpha t}. \tag{5}$$

The strength of interaction is measured with the parameter g, whilst the exponential rise (and fall) rate of the synapse is equal to α, such that the maximal synaptic response occurs at a time α^{-1} after the arrival of an action potential. The step function $\Theta(x)$ in equation (4) is equal to one for $x > 0$ and vanishes for $x \leq 0$. In the steady periodic firing state defined by $\lim_{k\to\infty} T_{k+1}^i - T_k^i \equiv \Delta$ (independent of initial conditions), the infinite sum in equation (4) can be reduced to a convergent geometric progression. In fact the input to neuron 2 (assuming that neuron 1 last fired at $t = 0$) takes the form $I_2(t) = I(t)$, where

$$I(t) = \frac{g\alpha^2 \mathrm{e}^{-\alpha(t-t_d)}}{(1 - \mathrm{e}^{-\alpha\Delta})} \left\{ (t - t_d) + \frac{\Delta \mathrm{e}^{-\alpha\Delta}}{(1 - \mathrm{e}^{-\alpha\Delta})} \right\}, \quad t \in [t_d, t_d + \Delta). \tag{6}$$

We now introduce a phase θ, $0 \leq \theta \leq 1$, such that if neuron 1 fires at $t = T_k^1$ then neuron 2 fires at $T_k^2 = T_k^1 - \theta\Delta$, again at $T_{k+1}^2 = T_k^1 + \Delta(1 - \theta)$. This periodic behaviour is illustrated in figure 1. In this case $I_1(t) = I_2(t + \theta\Delta)$ and outside their ranges the $I_i(t)$ are periodic:

$$I_1(t + n\Delta) = I_1(t) \quad t \in [t_d - \theta\Delta, t_d + \Delta(1 - \theta)) \tag{7}$$

$$I_2(t + n\Delta) = I_2(t) \quad t \in [t_d, t_d + \Delta), \quad n \in \mathbb{Z}. \tag{8}$$

To find the phase θ and period Δ for steady state periodic behaviour we consider the simultaneous equations

$$\phi_1(\Delta) = h \qquad \phi_2(\Delta - \theta\Delta) = h. \tag{9}$$

For the membrane potentials $\phi_i(t)$, $i = 1, 2$ given by (3) and $I_i(t)$ given by (4), we may explicitly perform the integration in (9) and hence reduce equations (9) to a coupled system of algebraic equations. A simple condition on the phase and period is formed from the expression $G(\theta, \Delta) = \phi_1(\Delta) - \phi_2(\Delta - \theta\Delta) = 0$ where

$$G(\theta, \Delta) = \mathrm{e}^{-\Delta/\tau} \int_0^{\Delta} \mathrm{d}t' \mathrm{e}^{t'/\tau} [I(t' + \theta\Delta) - I(t' - \theta\Delta)]. \tag{10}$$

Two obvious phase solutions, from the periodic properties of $I(t)$, are the synchronised solution with $\theta = 0$ (or equivalently $\theta = 1$) and the anti–synchronous solution $\theta = 1/2$. Moreover, if θ is a solution, then $(1 - \theta)$ is also a solution. By manipulating the expression for $G(\theta, \Delta)$ it is possible to form the relation $\phi_2(\Delta - \theta\Delta) = h - G(\theta, \Delta)$. Suppose θ is slightly larger than a stable equilibrium value. Then neuron 2 should fire later to restore the correct value of θ. This requires that $\phi_2(\Delta - \theta\Delta)$ should be smaller than h or equivalently that $G(\theta, \Delta)$ should be an increasing function of θ near the equilibrium value. Otherwise a reset will occur causing a dramatic change in the network dynamics. Hence, the condition for stability of a solution is defined by

$$\frac{\partial G(\theta, \Delta)}{\partial \theta} > 0. \tag{11}$$

All numerical results are produced using the continuation and bifurcation software AUTO94 [32]. Although primarily written for ODEs, AUTO94 can compute solution branches for algebraic systems of the form (9), detect simple bifurcation points and compute bifurcating branches. Note that if (9) can not be reduced explicitly to an algebraic system then a numerical quadrature method (such as composite Simpson's rule) may be applied to approximate the algebraic system. The stability of the branches may be established by evaluating the inequality (11). However, AUTO94 can also perform the desired stability analysis.

In the numerical results that follow we have chosen a time scale such that $\tau = 1$ and the constants g and h are fixed with $g = 0.4$, $h = 0.25$. Pseudo–arclength continuation was performed either in α (with fixed t_d) or t_d (with fixed α), solving for the phase difference θ and period Δ in either case. It should be noted that on some of the branches in figures 2–6 bifurcations in Δ were also found, for given values of θ.

In figure 2 we plot the bifurcation diagram for the phase θ versus α in the presence of small delays and also for $t_d = 0$ (reproducing the results of Van Vreeswijck *et al* [18]). For small values of the synaptic rate constant α there are two possible states showing either complete synchrony, $\theta = 0, 1$, or complete anti–synchrony, $\theta = 1/2$. Only the anti–synchronous state is stable. With increasing α, corresponding to progressively faster synapses, there is a pitchfork bifurcation at a critical value of $\alpha = \alpha^c$ and two additional equilibria are born. The anti–synchronous solution loses stability and continues as an unstable branch. The two new states are stable and have intermediate phases i.e. are neither synchronous nor anti–synchronous and are referred to as asynchronous. As $\alpha \to \infty$ the α–function approximates a Dirac δ pulse and the stable asynchronous solutions approach closely to the perfectly synchronised solution (at $\theta = 0$ or $\theta = 1$). For small delays ($t_d \leq 0.25$), once again there is a pitchfork bifurcation from a stable anti–synchronous solution leading to the creation of two new stable states for some critical α. An increase in t_d causes further desynchronisation in the sense that the critical value for α increases and for a fixed $\alpha > \alpha^c$ the solution branches move inward toward the anti–synchronous solution. In figures 3, 4, 5 and 6 we show bifurcation diagrams for θ vs t_d with several different α values. Figure 3, with $\alpha = 3 < \alpha^c$ (for $t_d = 0$), shows that for small t_d the anti–synchronous solution is the only stable one. Increasing t_d leads to the creation of two new unstable branches which eventually co–exist with the synchronous solution. This phenomenon of bifurcation and approach to the synchronous solution is repeated at larger values of t_d but with an interchange of solution stabilities. For a fixed phase θ, this leads to an alternating sequence of stable and unstable solutions with increasing t_d. In figures 4 and 5 we show behaviour in the phase θ as the delay t_d varies in the regime $\alpha > \alpha^c$ (for $t_d = 0$). For small t_d, figure 4, with $\alpha = 5$, simply re–expresses the results shown in figure 2 to the right of the largest value of α^c. Note that as t_d is increased from zero the desynchronisation effect becomes complete in the sense that the stable intermediate phase solutions join with the anti–synchronous solution at $t_d \sim 0.4$. Beyond this point the anti–synchronous solution becomes stable. Furthermore, two new stable solutions are born which approach the synchronous state with a further increase in t_d.

As can be seen from both figures 4 and 5 a host of other solutions are born with increasing t_d. Moreover, the possibility exists for multiple synchronous and anti–synchronous solutions to exist with differing periods and stabilities. Note that for $\alpha \leq 5.85$ (figures 2, 3, 4, 5) AUTO94 detected the bifurcations along the $\theta = 1/2$ branch, whereas for $\alpha > 5.9$ no bifurcations were detected following this branch. However the bifurcating branches persist for $\alpha > 5.9$, as is evident from figure 6. This figure was formed by using continuing points on the branches in figure 5 in α up to $\alpha = 10$ and then continuing each branch in the time–delay t_d.

Recently Ernst *et al* [23] and Mather and Mattfeldt [24] have analysed the effect of propagation delays, in a similar system to that considered, communicating via strict Dirac δ pulses. For excitatory couplings both conclude that for $t_d < \Delta/2$ two new stable phase solutions are possible, supporting the idea that propagation delays can induce desynchronisation. By taking a sufficiently large value of α it is possible to make an interesting comparison with this work. In figure 6 we explore the *pulsed* regime by setting $\alpha = 10$ and construct the θ vs t_d bifurcation diagram for $\theta \geq 1/2$ (solutions with $\theta < 1/2$ are easily generated by symmetry). For small t_d we see, as expected, that the synchronous solution ($\theta = 0, 1$) is stable whilst the anti–synchronous ($\theta = 1/2$) one is unstable. With increasing t_d the anti–synchronous solution remains unstable, whilst an initially stable synchronous solution desynchronises with increasing t_d. At $t_d \simeq \Delta/2$, ($t_d \simeq 0.31$), a stable solution is born from $\theta = 1/2$ that eventually approaches the synchronous state with a further increase in t_d. Furthermore, as before, other solutions are created with increasing t_d. In fact in this pulsed regime ($\alpha \to \infty$) with $t_d < \Delta/2$ our results are in agreement with those of Ernst *et al* and Mather and Mattfeldt [24]. However, in the regime where their analysis does not apply ($t_d \geq \Delta/2$) we see the creation of new solutions and multiple mixed stability synchronous and anti–synchronous solutions. For very large t_d all solutions approach either the synchronous or anti–synchronous states, both of which possess stable solutions for some period Δ. Note that multi–stable dynamical systems have important applications as pattern recognition and memory storage devices. Indeed, the conditions under which time–delayed recurrent loops of integrate–and–fire neurons exhibit multi–stability has recently been investigated [37].

III. SHUNTING SYNAPTIC CURRENTS

In real neurons synaptic input currents depend upon the deviation of the cell membrane voltage from some resting potential. The post–synaptic current is in fact mainly due to localised conductance changes for specific ions and a realistic form for it involves voltage dependencies in the form of shunts. To model this we let the membrane dynamics evolve according to the ODEs:

$$\frac{\mathrm{d}\phi_i}{\mathrm{d}t} = -\frac{\phi_i}{\tau} + I_i(t)(s - \phi_i), \quad 0 < \phi_i(t) < h, \quad i = 1, 2 \tag{12}$$

with the reset conditions (2) of section II. The membrane reversal potential (measured with respect to the resting potential of the neuron), s, is positive for an excitatory synapse and negative for an inhibitory one. Once again, we may construct a system of two pulse–coupled neurons with the input $I_i(t)$ to neuron i given by a sum of delayed α–functions (4). In the periodic steady firing state, the membrane potential ODEs may be written (after shifting them to the same time frame)

$$\frac{\mathrm{d}\phi_i}{\mathrm{d}t} = A_i(t)\phi_i + F_i(t), \quad t \in (0, \Delta) \tag{13}$$

with

$$A_i(t) = -\frac{1}{\tau} - I(t + \eta_i\theta\Delta), \quad F_i(t) = sI(t + \eta_i\theta\Delta) \tag{14}$$

and $I(t)$ is given by equation (6) with $\eta_1 = +1$ and $\eta_2 = -1$. The quantities $A_i(t)$ may be interpreted as time dependent cell membrane decay functions. The solution of (13) is given by

$$\phi_i(t) = \int_0^t \left(\exp \int_{t'}^t A_i(t'')\mathrm{d}t'' \right) F_i(t')\mathrm{d}t'. \tag{15}$$

The solution of

$$\phi_i(\Delta) = h, \qquad i = 1, 2 \tag{16}$$

determines the phase θ and period Δ for steady state periodic behaviour. As in section II the stability of solutions is determined with equation (11) where $G(\theta, \Delta) = \phi_1(\Delta) - \phi_2(\Delta) = 0$.

Note that due to the form of the $\phi_i(t)$, each of the equations in (16) is in fact an integral equation. The use of numerical quadrature allows the reduction of the two integral equations to two nonlinear algebraic ones. For the purposes of this section a standard composite Simpson's rule was chosen for evaluation of all integrals. All remaining parameters are as in section II. For zero delay we find a pitchfork bifurcation in the phase θ with an increasing shunt parameter s (and fixed α). These results are detailed in a companion paper [30]. Interestingly, shunts act to limit the firing frequency of the system, and may play a role in suppressing activity in large neural populations [38]. For small delays ($t_d < 0.075$) the bifurcation point and shape of this branch does not vary significantly from the zero delay case. The shape of this solution branch is essentially that seen in figure 7 for $s > 0.95$. However, in the presence of small delays several new solutions are created for lower values of s as shown in figure 7. In figure 8 we show the corresponding bifurcation diagram for the period Δ with variation in s. Larger delays lead to a more complex and interesting bifurcation picture. The bifurcation diagram figure 9 clearly demonstrates that larger delays can lead to the existence of multiple stable asynchronous solutions ($1 < s < 1.75$). Note that for s less than some critical value the system fails to oscillate since the threshold condition for firing can never be reached in this particular parameter regime. A further interesting feature that cannot be shown in the representation of figure 9 is that for a large range of s there are multiple synchronous and anti–synchronous solutions, differing in period and stability. To reveal this very rich structure we present a three dimensional view of the phase and period of solutions as a function of α in figure 10. The multiplicity of solutions is apparent in this figure and is easier to visualise when one can appreciate the existence of three distinct groups of solution branches, each possessing a different bifurcation structure. Note that the solutions with $\theta = 0, 1/2, 1$ always exist, for some Δ, even if they are not shown in figure 10.

IV. ELECTRICAL AND CHEMICAL COUPLING

In addition to chemical synapses, there are many examples of direct electrical connections between cells. These connections occur via channels that span the pre and postsynaptic membranes and are called *gap junctions*. Electrical synapses are present in many invertebrate nervous systems such as the gastric CPG of the previously mentioned crab. For CPGs found in invertebrates with small numbers of neurons it is common to find reciprocal inhibition between bursting neurons in conjunction with electrical coupling. Interestingly, electrical synapses have recently been found in a simple vertebrate, namely between motor–neurons in the spinal cord of the Xenopus tadpole [39]. Hence, dynamics of coupled neuronal oscillators including direct electrical connections may have a role in determining the functional significance of gap junctions.

As before we consider the evolution of the membrane potential $\phi_i(t)$, $i = 1, 2$ for two identical pulse–coupled integrate–and–fire neurons, firing periodically (of period Δ). We now incorporate the effects of a bi–directional gap junction. To describe the dynamics (illustrated in figure 11), it is convenient to introduce the following notation:

$$\phi_i(t + T^j) = \phi_{ij}(t) \quad t \in (0, \tilde{\Delta}_j), \quad i, j = 1, 2 \tag{17}$$

where T^j denotes the time that neuron j last fired, $\tilde{\Delta}_1 = \Delta(1 - \theta)$ and $\tilde{\Delta}_2 = \theta\Delta$. The total period $\Delta = \tilde{\Delta}_1 + \tilde{\Delta}_2$. The reset conditions, (2), become

$$\lim_{\epsilon \to 0_+} \phi_i(T^i + \epsilon) = \phi_{ii}(0) = 0 \quad i = 1, 2 \tag{18}$$

$$\lim_{\epsilon \to 0_+} \phi_i(T^i - \epsilon) = \phi_{ij}(\tilde{\Delta}_j) = h \quad i, j = 1, 2 \quad i \neq j. \tag{19}$$

From Kirchoff's law the cell membrane potentials evolve according to

$$\frac{\mathrm{d}\phi_{ij}}{\mathrm{d}t} = -\frac{\phi_{ij}}{\tau} + \sigma(\phi_{\bar{i}j} - \phi_{ij}) + I_i(t + \eta_i\theta\Delta) \quad t \in (0, \tilde{\Delta}_j) \tag{20}$$

with $\bar{i} = 1$ if $i = 2$ and vice versa, $\eta_1 = 0$ and $\eta_2 = -1$. The parameter $\sigma = 1/(rC)$ incorporates the resistance r of the electrical synapse between the two neurons and reflects

the strength of electrical coupling. Note that the effect of reset is communicated between neurons due to this coupling and gives rise to the discontinuous evolution of cell membrane potentials over a whole period Δ (as shown in figure 11). For simplicity we drop all discussion of discrete time–delays and set $t_d = 0$. However, their effects may be incorporated with the method used in section 2 and 3 if one so wishes. Once again the variation of parameters formula may be used to write a solution as

$$\phi_i(t) = \mathrm{e}^{-\epsilon t}\phi_{ij}(0) + \int_0^t \mathrm{e}^{-\epsilon(t-t')}[I_i(t' + \eta_i\theta\Delta) + \sigma\phi_{\bar{i}j}(t')]\mathrm{d}t', t \in (0, \tilde{\Delta}_j) \tag{21}$$

where $\epsilon = \tau^{-1} + \sigma$. Hence, by substitution of (21) into (20), we may form the integro-differential equation

$$\frac{\mathrm{d}\phi_{ij}}{\mathrm{d}t} = -\epsilon\phi_{ij} + \int_0^t H(t-t')\phi_{ij}(t')\mathrm{d}t' + F_{ij}(t) \tag{22}$$

where $H(t) = \sigma^2\mathrm{e}^{-\epsilon t}$ and

$$F_{ij}(t) = I_i(t + \eta_j\theta\Delta) + \sigma\mathrm{e}^{-\epsilon t}\phi_{\bar{i}j}(0) + \sigma\int_0^t \mathrm{e}^{-\epsilon(t-t')}I_{\bar{i}}(t' + \eta_j\theta\Delta)\mathrm{d}t'. \tag{23}$$

Thus, between resets, the $\phi_{ij}(t)$ evolve according to a linear Volterra integral–differential equation. Each neuron behaves like the original integrate–and–fire neuron of section II, but with an external input $F_{ij}(t)$ (instead of just $I_i(t)$) and an additional feedback contribution that takes into account electrical coupling via the gap junction. The feedback transfer function is $H(t)$. A unique solution of the model may be constructed that generalises that of sections II and III. Since both the convolution kernel $H(t)$ and the function $F_{ij}(t)$ are continuous on $(0, \tilde{\Delta}_j)$ we can apply the following result due to Burton [40]. If $Z(t)$ is the solution of the homogeneous equation

$$\frac{\mathrm{d}Z}{\mathrm{d}t} = -\epsilon Z + \int_0^t H(t-t')Z(t')\mathrm{d}t', \qquad Z(0) = 1 \tag{24}$$

and if $\phi_{ij}(t)$ is a solution of equation (22) on $(0, \tilde{\Delta}_j)$ then

$$\phi_{ij}(t) = Z(t)\phi_{ij}(0) + \int_0^t Z(t-t')F_{ij}(t')\mathrm{d}t'. \tag{25}$$

Hence, $\phi_{ij}(t)$ is uniquely determined by the initial condition $\phi_{ij}(0)$ together with a variation of parameters solution (25). With the use of Laplace transforms and the Bromwich theorem, equation (24) may be solved as

$$Z(t) = \frac{1}{2}(\mathrm{e}^{\epsilon_+ t} + \mathrm{e}^{\epsilon_- t}) \tag{26}$$

where $\epsilon_\pm = -\epsilon \pm \sigma$. We may now self–consistently solve the equations for the somatic potentials to determine both the phase θ and period Δ in the steady state. Simultaneously solving $\phi_{11}(\Delta(1-\theta)) = X_1$, $\phi_{22}(\theta\Delta) = X_2$, $\phi_{12}(\theta\Delta) = h$ and $\phi_{21}(\Delta(1-\theta)) = h$, yields the unknowns $\theta, \Delta, \phi_{12}(0)$ and $\phi_{21}(0)$, where $X_{1,2}$ must be determined self–consistently with $X_{1,2} < h$. Numerically we apply numerical quadrature to reduce these equations to an algebraic system. As before, we construct the function $G(\theta, \Delta)$ as

$$G(\theta, \Delta) = \phi_{12}(\theta\Delta) - \phi_{21}(\Delta(1-\theta)) = 0. \tag{27}$$

The condition for stability is $\partial G(\theta, \Delta)/\partial\theta > 0$. Note that in the limit of no electrical coupling $\sigma \to 0$ we recover the solutions for the somatic potentials given in section II.

In figure 12 we plot the variation of relative phase θ as a function of the strength of electrical interaction σ for a restricted set of parameters, namely $\alpha = 5.5$, $X_1 = 6.58 \times 10^{-2}$, $X_2 = 9.94 \times 10^{-2}$, $\phi_{12}(0) = 1.28 \times 10^{-3}$ and $\phi_{21}(0) = 4.08 \times 10^{-2}$ with all remaining parameters as in section II. It appears from numerical experiments that new solutions can not be created but rather that weak coupling can favour nearly anti–synchronous phase relationships, whilst strong electrical coupling can increase the synchrony of solutions. More interesting is the observation that small changes in the strength of electrical coupling can lead to sharp changes in the period of oscillation. This can be seen in figure 13 for the corresponding plot of figure 12 for variation of the period Δ with σ. Such an effect has also been observed for asynchronous periodic rhythms generated in a similar system of two chaotic neurons [41]. From a functional point of view the mixture of electrical and chemical coupling provides a high sensitivity for period regulation of the asynchronous periodic state.

V. EFFECTS OF DENDRITIC STRUCTURE

In general, the diffusive nature of dendrites means that the single neuron somatic response is a convolution of the synaptic input with the response function of the dendritic tree. Furthermore, the precise ordering of the axonal fibre system in cortical regions suggest that the synaptic locations of inputs play a role in circuit function [42]. Rospars and Lansky [43] have described the response of a compartmental model in which it is assumed that dendritic potentials evolve without any influence from the nerve impulse generation process. However, the electrical coupling between the soma and dendrites means that there is a feedback signal across the dendrites whenever the somatic potential resets. This situation is described in detail by Bressloff [44]. The basic idea is to eliminate the passive component of the dynamics (the dendritic potential) to yield a Volterra integro–differential equation for the somatic potential. An iterative solution to the integral equation can be constructed in terms of a second order map of the firing time, in contrast to a first order map as found in models lacking dendritic structure [45]. Unfortunately, a description of two pulse–coupled compartmental models with reset is analytical unwieldy, although some work on this problem has been done by Crook [27]. However, substantial progress can be made by considering the dendritic tree of a neuron to be idealised as a semi–infinite one–dimensional cable [46] . Furthermore, it is illuminating to work in the *phase*–interaction representation, rather than the *pulse*–interaction picture used up till now. This can be achieved using the formalism developed by Kuramoto and others [7,18] and, in this particular instance, helps to isolate the contribution of dendritic structure to neuronal synchronisation. We show that the synchronous solution can change from stable to unstable as the point of synaptic input moves further from the soma (see figure 14). Independent work by Crook [27] on cells connected by synapses at the ends of finite dendritic cables (with variable space constant) reinforces these results. Both Crook [27] and Bressloff and Coombes [28] propose that this mechanism may be used by neural circuits, whereby proximal connections encourage synchrony and more distal encourage asynchrony or anti-synchrony.

In general, cell membrane properties are such that there is a nonlinear relationship between membrane ionic current and the transmembrane potential [34,47]. In fact a more realistic scenario, than so far considered, is given by the equations (for $i = 1, 2$)

$$\frac{\partial V_i(\xi,t)}{\partial t} = D\frac{\partial^2 V_i(\xi,t)}{\partial \xi^2} - \frac{V_i}{\tilde{\tau}} + E_i(\xi,t) \tag{28}$$

$$\frac{\mathrm{d}\phi_i}{\mathrm{d}t} = f(\phi_i) + \rho_0[V_i(0,t) - \phi_i(t)], \quad 0 < \phi_i(t) < h. \tag{29}$$

Equation (28) is the standard cable equation for the dendritic potential $V_i(\xi,t)$ of an unbranched dendrite on neuron i, with dendritic coordinate $\xi \in \mathbb{R}^+$. The decay constant $\tilde{\tau}$ and the diffusion constant D may be related to underlying cellular properties of dendritic tissue and in the following analysis we fix length and time scales by setting $D = \tilde{\tau} = 1$. The soma is considered to be sited at position $\xi = 0$ on the cable and $\mathcal{I}_i(t) = \rho_0[V_i(0,t) - \phi_i(t)]$ is the current density flowing to the soma from the cable. The equation for the dendritic potential $V_i(\xi,t)$ has input $E_i(\xi,t)$ representing the synaptic input, taken to be absent at the soma. Equation (28) is supplemented by the boundary condition $-\partial V_i/\partial\xi|_{\xi=0} = \mathcal{I}_i(t)$. Equation (29) (without the ρ_0 dependent coupling term) for the somatic potential $\phi_i(t)$ of a neuron was originally proposed by Abbott and Kepler [48] through a systematic reduction of the Hodgkin–Huxley equations. Furthermore, they have shown using experimental data that $f(\phi)$ can be fitted with a cubic [48]. In order to simplify our analysis, we shall assume that the current flowing from the soma to the dendrite is negligible, which amounts to imposing the homogeneous boundary condition $\partial V_i/\partial\xi|_{\xi=0} = 0$. After absorbing a term $-\rho_0\phi_i$ into the definition of the function $f(\phi_i)$ in equation (29) we have that $\mathcal{I}_i(t)$ is transformed to $\rho_0 V_i(0,t)$. We now solve equation (28) for $V_i(\xi,t)$ in terms of the synaptic inputs and set $\xi = 0$ to give

$$\mathcal{I}_i(t) = 2\rho_0 \int_{-\infty}^{t} \mathrm{d}t' \int_0^{\infty} \mathrm{d}\xi' K(\xi', t-t') E_i(\xi', t') \tag{30}$$

where $K(\xi,t) = \mathrm{e}^{-t-\xi^2/4t}/\sqrt{4\pi t}$ is the response or Green's function of the infinite cable equation. For concreteness we consider synaptic input on the cable to impinge at location

ξ_0 only such that

$$E_i(\xi, t) = \delta(\xi - \xi_0) I_i(t) \tag{31}$$

where $I_i(t)$ has the form of equation (4).

The analytical intractability of this model is much reduced with the aid of averaging techniques valid in the limit of weak coupling. Indeed a nonlinear transform may be used to study nonlinear integrate–and–fire neurons in the framework of *pulse–coupled phase models* [8]. In the uncoupled state each identical neuron is imagined to fire with a natural period Δ at times $-\theta_i \Delta$. Weak coupling of the two neurons will induce some relative phase relationship. The dynamical variable of interest in the weak–coupling regime is the phase of each oscillator. Specifically, following [18] one can apply the following nonlinear transform to equation (29):

$$\theta_i(t) + \frac{t}{\Delta} = \psi(\phi_i(t)) \equiv \frac{1}{\Delta} \int_0^{\phi_i(t)} \frac{\mathrm{d}\phi'}{f(\phi')} \tag{32}$$

with $\Delta = \int_0^h \mathrm{d}\phi'/f(\phi')$. The phase variables θ_i satisfy

$$\frac{\mathrm{d}\theta_i}{\mathrm{d}t} = J(t/\Delta + \theta_i)\mathcal{I}_i(t) \qquad t \in (-\theta_i\Delta, (-\theta_i + 1)\Delta) \tag{33}$$

where $J(z) = \Delta^{-1}/[f \circ \psi^{-1}(z)]$, and $J(z + n) = J(z)$, $n \in \mathbb{Z}$. Neuron i fires when $\phi_i = h$ or equivalently, from (32), when $\theta_i + t/\Delta = n$ for integer n. The corresponding firing times are $t = (n - \theta_i)\Delta$ and hence

$$I_i(t) = I(t + \theta_j \Delta) \quad t \in [-\theta_j\Delta, (-\theta_j + 1)\Delta) \tag{34}$$

where $I(t)$ is given by equation (6) and $I(t + n\Delta) = I(t)$. However, to simplify matters further still we shall drop discussion of transmission delays by setting $t_d = 0$ and ignore the shape of post–synaptic currents so that $I(t) = g \sum_n \delta(t - n\Delta)$. Now assume that the term t/T varies much more quickly than either of the $\theta_i(t)$ which is true for weak coupling. Then we can average the right side of (33) over one period Δ and substitute equations (30), (31) and (34) to obtain

$$\frac{\mathrm{d}\theta_i}{\mathrm{d}t} = \mathcal{H}(\theta_j - \theta_i) \tag{35}$$

with

$$\mathcal{H}(\theta) = g \int_0^\infty \mathrm{d}t J(t-\theta) K(\xi_0, t\Delta) \tag{36}$$

and we have absorbed the factor of $2\rho_0$ within the coupling strength g. As discussed in [18], the function $J(t)$ is the phase interaction function of the model in the case of an instantaneous synapse. The function $\mathcal{H}(\theta)$ involves the convolution of the instantaneous interaction function $J(t)$ with the dendritic response function $K(\xi_0, t)$ which depends explicitly on the location ξ_0 of the synapse on the dendritic cable. It follows that $\mathcal{H}(\theta)$ can be written as a function of the phase difference, $\theta = \theta_1 - \theta_2$, by invoking the periodicity properties of $J(t)$ and $I(t)$. The evolution of the phase difference may now be written

$$\frac{\mathrm{d}\theta}{\mathrm{d}t} = -\mathcal{G}(\theta), \quad \mathcal{G}(\theta) = \mathcal{H}(\theta) - \mathcal{H}(-\theta) \tag{37}$$

Solutions can be found by solving equation (37) for θ in the steady state, $\mathcal{G}(\theta) = 0$, with Δ given by (32). Solutions are stable if $\partial\mathcal{G}(\theta)/\partial\theta > 0$. Since $\mathcal{H}(\theta)$ is periodic with period 1, $\mathcal{G}(\theta)$ always has zeros at $\theta = 0, 1/2, 1$. For simplicity, we shall take $J(t) = -\sin 2\pi t$, which is known to be a good approximation when f of equation (29) has an experimentally determined form [19]. Using the following Fourier representation of the fundamental cable solution: $K(\xi_0, t) = (2\pi)^{-1} \int_{-\infty}^{\infty} \mathrm{d}k \mathrm{e}^{ik\xi_0 - \epsilon(k)t}$, where $\epsilon(k) = k^2 + 1$, the stability function $\mathcal{G}(\theta)$ becomes

$$\mathcal{G}(\theta) = g \sin(2\pi\theta) \int_{-\infty}^{\infty} \frac{\mathrm{d}k}{2\pi} \mathrm{e}^{ik\xi_0} A(k) \tag{38}$$

with

$$A(k) = \frac{\epsilon(k)}{\epsilon(k)^2 + \omega^2}, \quad \omega = \frac{2\pi}{\Delta}. \tag{39}$$

Hence, stability is partly dependent upon whether $\widehat{A} = \int_{-\infty}^{\infty} \mathrm{d}k \mathrm{e}^{ik\xi_0} A(k) > 0$. The integral $\widehat{A}$ can be evaluated by closing the contour in the upper–half complex k–plane as

$$\widehat{A} = \frac{\pi}{r} \mathrm{e}^{-r\xi_0 \cos(\beta/2)} [r\xi_0 \sin(\beta/2) + \beta/2] \tag{40}$$

with $r^2 = \sqrt{1+\omega^2}$ and $\tan\beta = \omega$, $0 \leq \beta \leq \pi/2$. We deduce from figure 15 that as the distance ξ_0 of the synapse from the soma increases from zero, $\widehat{A}$ reaches a critical value where a change in solution stability can occur. Increasing ξ_0 still further produces alternating bands of stability and instability for solutions to $\mathcal{G}(\theta) = 0$. In fact, the synchronous state ($\theta = 0, 1$) is stable for $\widehat{A} > 0$ and the anti–synchronous state ($\theta = 1/2$) is stable for $\widehat{A} < 0$ for excitatory coupling ($g > 0$). A similar checker–board structure of stable/unstable solutions with increasing axonal communication delay is seen in figures 3–6. Hence, ξ_0 plays an analogous role to that of a time delay, since the time of maximal response at the soma due to an input at ξ_0 increases with ξ_0. Interestingly this *time–to–peak* can be as large as a few 100 msec whereas axonal delays are typically 1–10 msec.

VI. DISCUSSION

The nonlinear dynamics of populations of pulse–coupled neuron models is of great importance in modelling the generation of biological rhythms. In general, neuronal pools can produce both anti-synchronous, asynchronous as well as synchronous firing patterns. Hence, identifying the biological features that lead to such behaviours is important. In this paper we have focused on a very simple model of a central pattern generator (CPG) built from two pulse–coupled integrate–and–fire neurons. The inclusion of simple measures of axonal propagation delay, shunting synaptic currents, the pulse–shape of such currents and electrical synapses can all be analysed using elementary analysis in conjunction with numerical techniques for constructing bifurcation diagrams. The inclusion of a dendritic structure complicates such an approach, yet it is a vital component of most single neuron anatomies. However, the spatio–temporal filtering properties of dendrites can be isolated with a reduction of the model, valid for intrinsically oscillating weakly coupled neurons. Moreover, such a reduced model is exactly solvable. By maintaining contact with neurophysiological reality both discrete and distributed delays arise naturally within the model CPG circuit description. Indeed, the rate of synaptic response (linked to the opening and closing of

ion channels) allows the possibility of asynchronous periodic rhythms for sufficiently slow synapses ($\alpha \sim O(1)$ with $\tau = 1$), whilst the synchronous state is prefered for instantaneous synapses. Another form of distributed delay arises from the diffusive nature of a passive dendritic tree since the *time–to–peak* of a signal depends on the distance of synaptic input from the soma. For some ranges of distance of the synapse from the soma the synchronous state can be destabilised in favour of an anti–synchronous periodic rhythm. The more obvious delays inherent to many neuronal interacting neuronal systems come in the form of communication delays. Not only can these discrete delays lead to stable asynchronous solutions for fast synaptic responses, they allow the formation of multiple stable periodic orbits with the same phase but differing period. Hence, their obvious importance in the construction of memory devices [37]. An interesting issue arises concerning transitions between these attractors and will be addressed elsewhere. Moreover, delays of the above type have other important consequences in larger systems than considered here. Interestingly, if the effective communication delay between neurons in a one–dimensional array of weakly–coupled integrate–and–fire neurons is sufficiently large, then the synchronous state can be destabilised in favour of a state of stable travelling waves. This picture is valid when effective somatic responses are *fast* compared to the natural frequency of neuronal oscillation, but is altered in the presence of say slow synapses or dendritic structure as expected from the results presented here (see [29] for further discussion). The distributed and discrete delays arising naturally in neuronal systems may therefore be responsible for the oscillatory waves observed in such structures as the olfactory cortex where distributed delays arise from both synaptic and dendritic properties and discrete delays arise from the large axonal separations between neurons [27,28]. The presence of realistic forms of voltage–dependent synaptic current with reversal potentials for specific ion channels has also been considered. Importantly, the cell membrane decay becomes a nonlinear function of time so that the steady state value of cell membrane potential can be reduced with an increase in the value of the (positive) reversal potential. Not only do stable asynchronous solutions arise through a pitchfork bifurcation (from the anti–synchronous state) with such an increase, but these so–called shunting

currents can act to limit the firing rate of the system. A more important source of control of the period of the system resides in the strength of electrical connections between neurons. The combination of synaptic and gap junctions is typical for many small CPG circuits found in invertebrates. The sharp variation of period with small change in strength of electrical coupling is also observed by Huerta *et al* [41], for the case of two coupled chaotic neurons, who suggest that the function of such a combination is to allow modulation of the period of asynchronous rhythms. Such a result highlights the importance of exploring the consequences of simple biological features in establishing rhythmic behaviour in coupled neuronal systems, since useful conclusions can be drawn about neurophysiological function. Finally, let us make the point that many CPG circuits are of the *half–center* [49] variety which rely upon reciprocal inhibition for rhythm generation rather than reciprocal excitation as considered here. In this case one requires extra physiological factors such as post-inhibitory rebound [50,51] or the inclusion of an external driving current for rhythm maintenance. In the case of a half–center oscillator with reciprocal inhibition and a sufficiently large external driving current (so that firing can occur in the absence of any coupling), bifurcation diagrams are qualitatively the same as those presented here, but with a reversal of stability for all solution branches.

ACKNOWLEDGEMENTS

The authors would like to thank Dr Paul Bressloff for helpful comments during the completion of this work. Both authors are supported by the applied nonlinear mathematics initiative of the EPSRC (UK). S Coombes is funded by grant number GR/K86220 and G J Lord by grant number GR/J97199 of the EPSRC (UK).

REFERENCES

[1] P. S. Katz and W. N. Frost, Trends in Neuroscience **19**, 54 (1996).

[2] J. M. Weimann, P. Meyrand, and E. Marder, Journal of Neurophysiology **65**, 111 (1991).

[3] A. I. S. R M Harris-Warwick, E Marder and M. Moulins, *Dynamical Biological Networks: The Stomatogastric Nervous System* (MIT Press, 1992).

[4] A. Roberts, Science Progress Oxford **74**, 31 (1990).

[5] Y. I. Arshavsky *et al.*, Trends in Neuroscience **16**, 227 (1993).

[6] W. Singer, in *The Handbook of Brain Theory and Neural Networks*, edited by M. A. Arbib (MIT Press, 1995), pp. 960–963.

[7] Y. Kuramoto, *Chemical oscillations, waves and turbulence* (Springer-Verlag, New-York, 1984).

[8] W. Gernster, Physical Review E **51**, 738 (1995).

[9] X. Wang and J. Rinzel, Neural Computation **4**, 84 (1992).

[10] F. K. Skinner, G. G. Turrigiano, and E. Marder, Biological Cybernetics **69**, 375 (1993).

[11] F. K. Skinner, N. Kopell, and E. Marder, Journal of Computational Neuroscience **1**, 69 (1994).

[12] N. Kopell and G. LeMasson, Proceedings of the National Academy of Science USA **91**, 10586 (1994).

[13] T. LoFaro, N. Kopell, E. Marder, and S. L. Hooper, Neural Computation **6**, 69 (1994).

[14] N. Kopell and D. Somers, Journal of Mathematical Biology **33**, 261 (1995).

[15] R. E. Mirollo and S. H. Strogatz, SIAM Journal of Applied Maths **50**, 1645 (1990).

[16] Y. Kuramoto, Physica D **50**, 15 (1991).

[17] J. J. Hopfield and A. V. M. Herz, Proceedings of the National Academy of Science USA **92**, 6655 (1995).

[18] C. van Vreeswijk and L. F. Abbott, Journal of Computational Neuroscience **1**, 313 (1994).

[19] D. Hansel, G. Mato, and C. Meunier, Europhysics Letters **23**, 367 (1993).

[20] A. Sherman and J. Rinzel, Proceedings of the National Academy of Science USA **89**, 2471 (1992).

[21] B. Mulloney, D. H. Perkel, and R. W. Budelli, Brain Research **229**, 25 (1981).

[22] S. K. Han, C. Kurrer, and Y. Kuramato, Physical Review Letters **75**, 3190 (1995).

[23] U. Ernst, K. Pawelzik, and T. Geisel, Physical Review Letters **74**, 1570 (1995).

[24] R. Mather and J. Mattfeldt, SIAM Journal of Applied Maths **56**, 1094 (1996).

[25] H. G. Schuster and P. Wagner, Progress of Theoretical Physics **81**, 939 (1989).

[26] E. Niebur, H. G. Schuster, and D. Kammen, Physical Review Letters **67**, 2753 (1991).

[27] S. M. Crook, Ph.D. thesis, University of Maryland, 1996.

[28] P. C. Bressloff and S. Coombes, Physical Review Letters (to appear) (1997).

[29] P. C. Bressloff and S. Coombes, International Journal of Modern Physics B (To appear) (1997).

[30] S. Coombes and G. J. Lord, Physical Review E **53**, R2104 (1996).

[31] W. Rall, in *Methods in neuronal Modelling*, edited by C. Koch and I. Segev (MIT Press, 1992), Chap. 2, pp. 9–62.

[32] E. Doedel, H. B. Keller, and J. P. Kernevez, International Journal of Bifurcation and Chaos **1**, 493 (1991).

[33] M. Tsodyks, I. Mitkov, and H. Sompolinsky, Physical Review Letters **71**, 1280 (1993).

[34] J. J. B. Jack, D. Noble, and R. W. Tsien, *Electric Current Flow in Excitable Cells* (Oxford Science Publications, 1975).

[35] L. F. Abbott and C. van Vresswijk, Physical Review E **48**, 1483 (1993).

[36] W. Gerstner and J. L. van Hemmen, Physical Review Letters **71**, 312 (1993).

[37] J. Foss, A. Longtin, B. Mensour, and J. Milton, Physical Review Letters **76**, 708 (1996).

[38] P. C. Bressloff and J. G. Taylor, Journal of Physics A **26**, L165 (1993).

[39] R. Perrins and A. Roberts, Journal of Neurophysiology **73**, 1005 (1995).

[40] T. A. Burton, SIAM Review **25**, 343 (1983).

[41] R. Huerta, M. I. Rabinovich, H. D. I. Abaranel, and M. Bazhenov, Physical Review E **55**, R2108 (1997).

[42] G. M. Shepherd, in *The Synaptic Organization of the Brain*, edited by G. M. Shepherd (Oxford University Press, 1990), pp. 3–31.

[43] J. P. Rospars and P. Lansky, Biological Cybernetics **69**, 283 (1993).

[44] P. C. Bressloff, Physica D **80**, 399 (1995).

[45] J. P. Keener, F. C. Hoppensteadt, and J. Rinzel, SIAM J. Appl. Math. **41**, 503 (1981).

[46] W. Rall, in *Methods in neuronal modelling*, edited by C. Koch and I. Segev (MIT Press, 1989), Chap. 2, pp. 9–96.

[47] D. Johnston and S. M. Wu, *Foundations of Cellular Neurophysiology* (MIT Press, 1995).

[48] L. F. Abbott and T. B. Kepler, in *Statistical Mechanics of Neural Networks*, No. 368 in *Lecture notes in Physics*, edited by L. Garrido (Springer-Verlag, 1990).

[49] R. L. Calabrese, in *The Handbook of Brain Theory and Neural Networks*, edited by

M. A. Arbib (MIT Press, 1995), pp. 444–447.

[50] S. Coombes and S. H. Doole, Dynamics and Stability of Systems **11**, 193 (1996).

[51] S. Coombes and S. H. Doole, Physical Review E **54**, 4054 (1996).

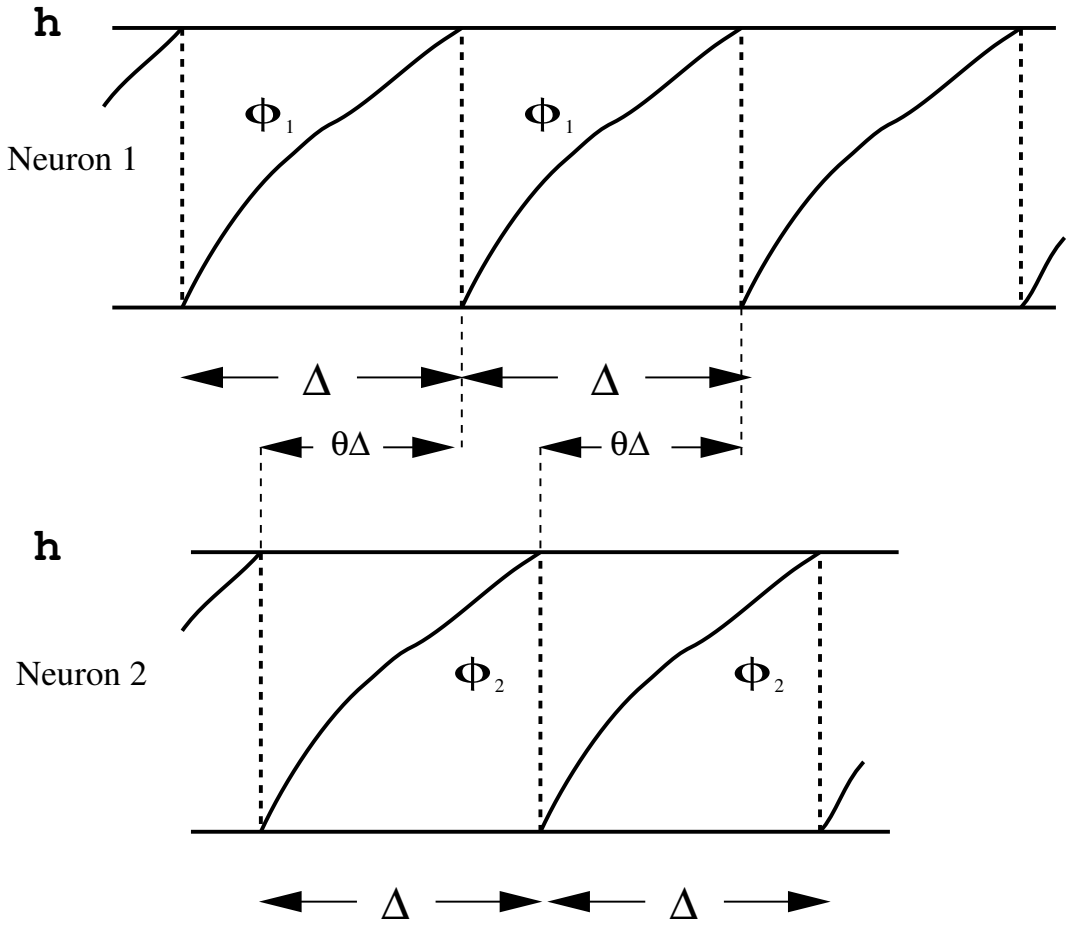

FIG. 1. Schematic diagram of the periodic solution for two pulse–coupled integrate–and–fire neurons with threshold h, period Δ and relative phase θ.

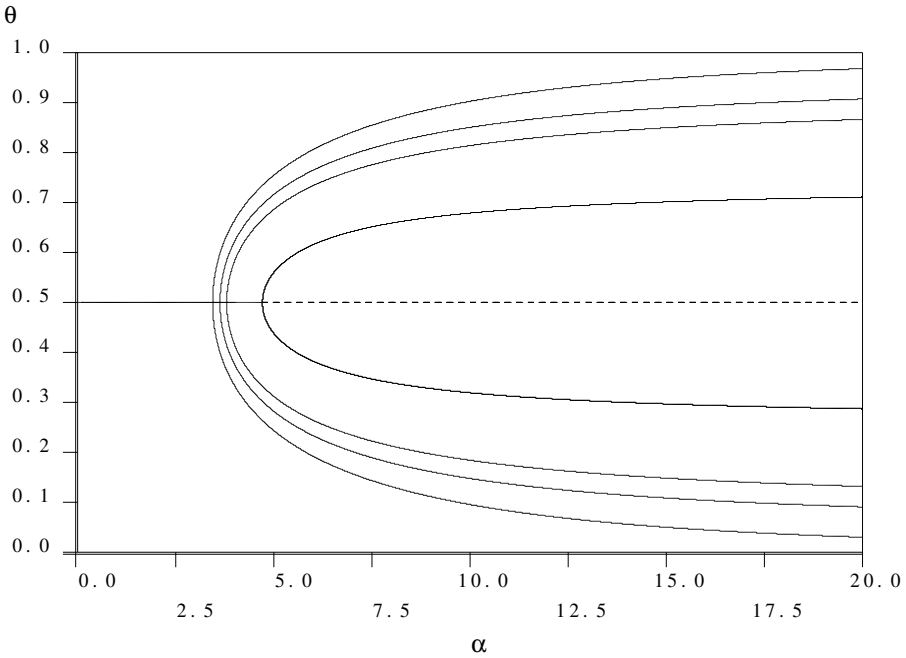

FIG. 2. θ vs α bifurcation diagram with $\tau = 1$ for varying delay times. The four branches above and below the anti–synchronous state ($\theta = 1/2$) correspond to four differing values of the time delay t_d. The branch bifurcating from $\theta = 1/2$ at the lowest value of α corresponds to the case with no delay, $t_d = 0$. Successive bifurcations for progressively larger α correspond to the case with delays, $t_d = 0.025$, $t_d = 0.05$ and $t_d = 0.25$ respectively. Solid (dashed) lines represent stable (unstable) solutions.

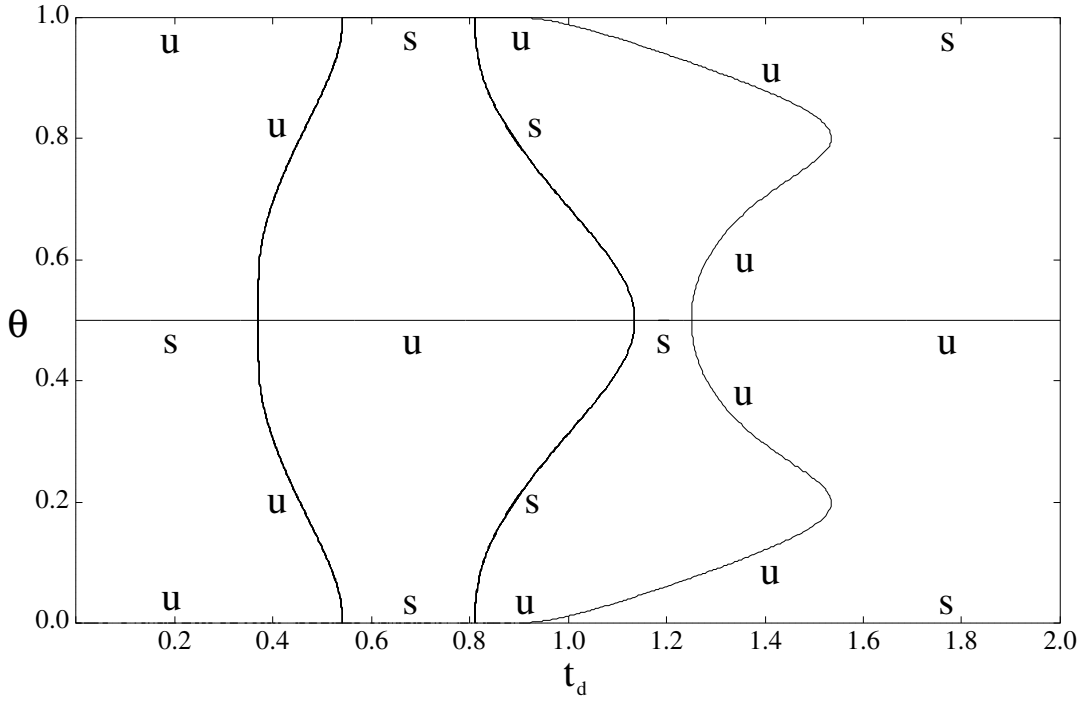

FIG. 3. θ vs t_d bifurcation diagram for $\alpha = 3$. Stable branches are denoted by **s** and unstable branches by **u**. Note the existence of multiple solutions with a fixed value of the phase difference θ and the checkerboard pattern of stable/unstable branches.

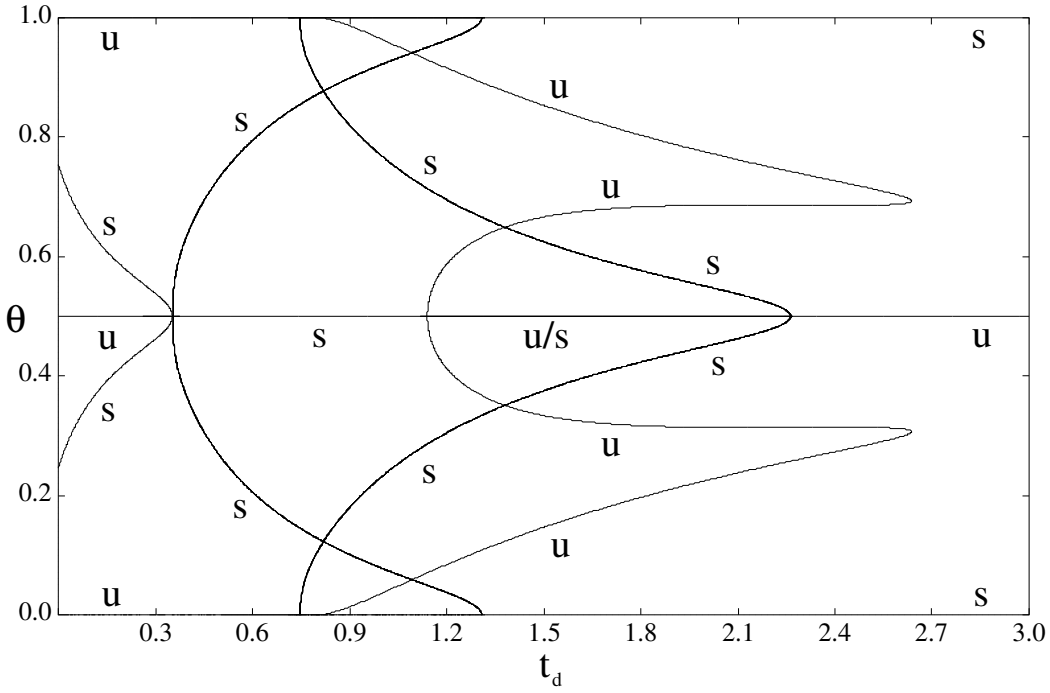

FIG. 4. θ vs t_d bifurcation diagram for $\alpha = 5$. Stable branches are denoted by **s** and unstable branches by **u**. Branches marked with **u/s** were found to be stable for one value of Δ and unstable for another.

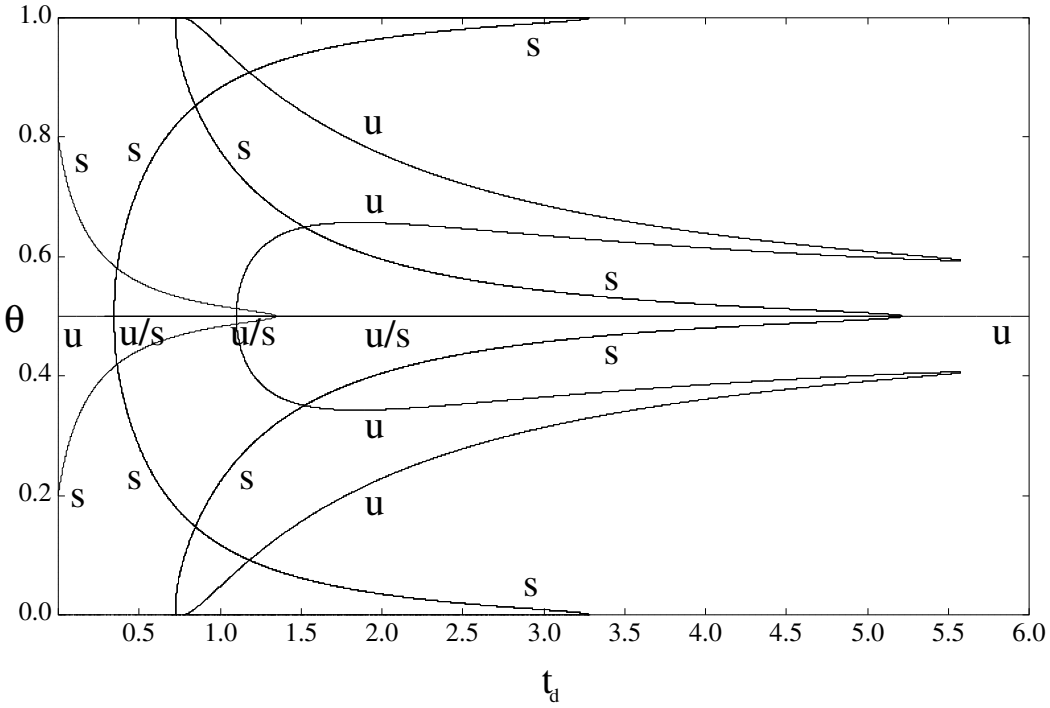

FIG. 5. θ vs t_d bifurcation diagram for $\alpha = 5.85$. Stable branches are denoted by **s** and unstable branches by **u**. Branches marked with **u/s** were found to be stable for one value of Δ and unstable for another.

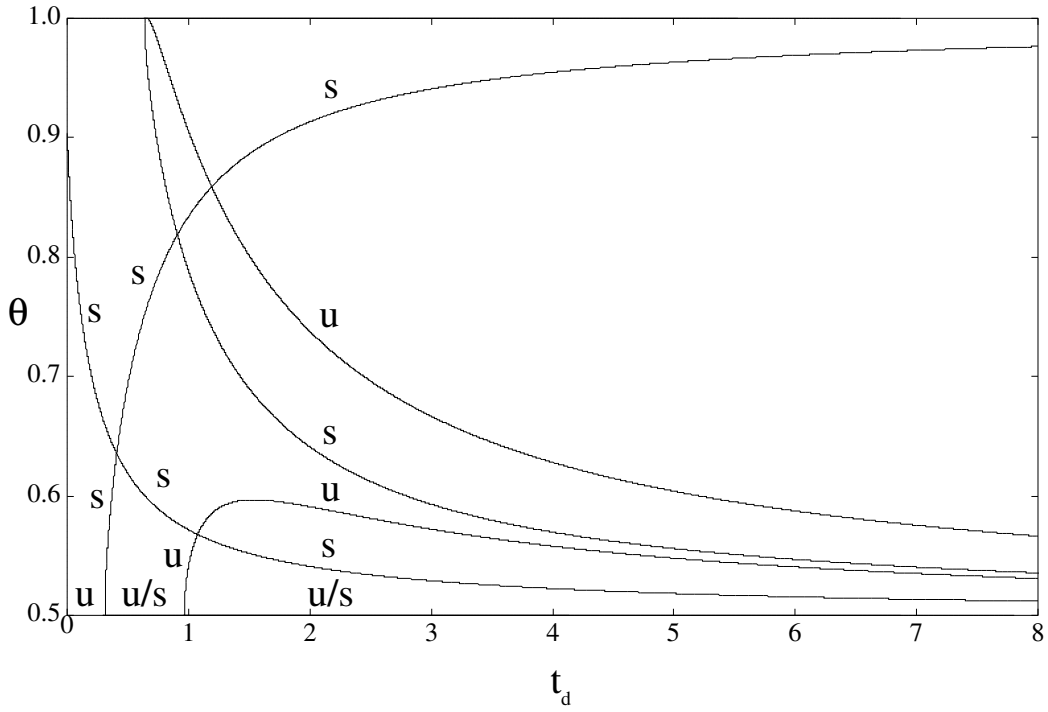

FIG. 6. θ vs t_d bifurcation diagram for $\alpha = 10$ (fast synaptic response). Stable branches are denoted by **s** and unstable branches by **u**. Branches marked with **u/s** were found to be stable for one value of Δ and unstable for another. Note that solutions with $\theta < 1/2$ may be generated by symmetry.

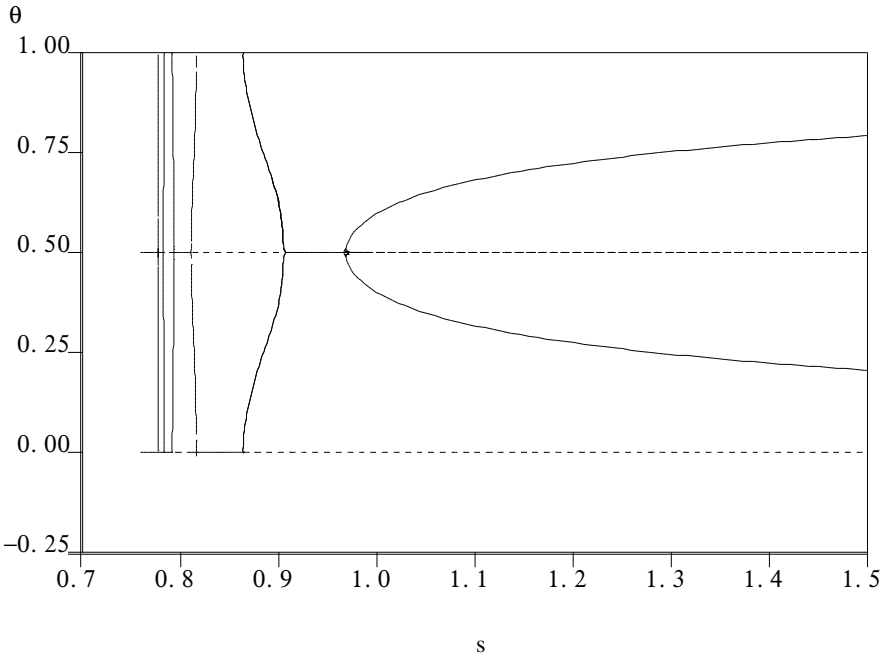

FIG. 7. θ vs s bifurcation diagram with $t_d = 0.012$ and $\alpha = 6$. Solid (dashed) lines indicate stable (unstable) solutions. solutions to the right of $s \sim 0.95$ are close to those in the zero delay case, $t_d = 0$. Solutions to the left of this point are created in the presence of a finite communication delay.

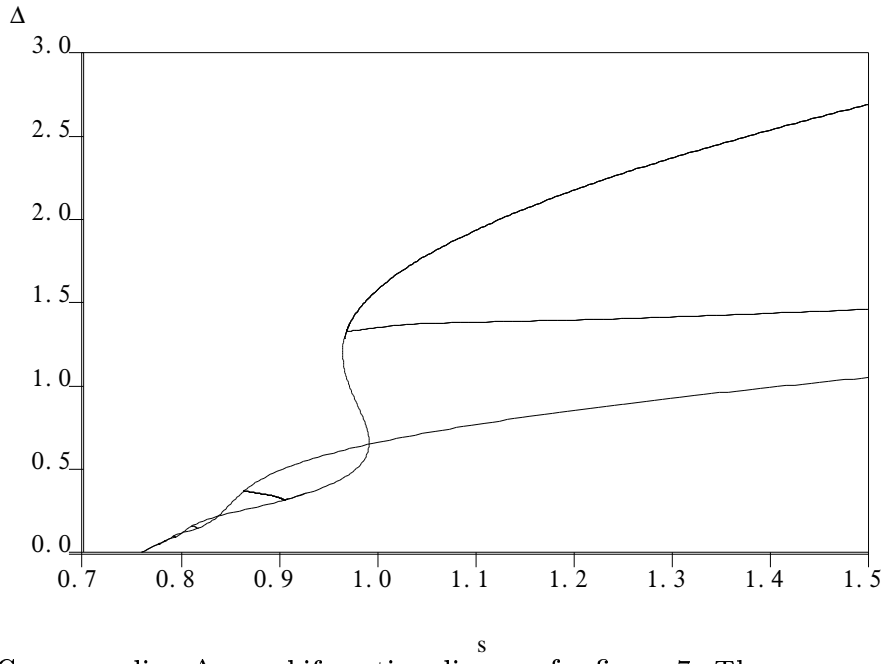

FIG. 8. Corresponding Δ vs s bifurcation diagram for figure 7. The upper, middle and lower branches on the right of the picture respectively correspond to the anti–synchronous, asynchronous and synchronous phase solutions.

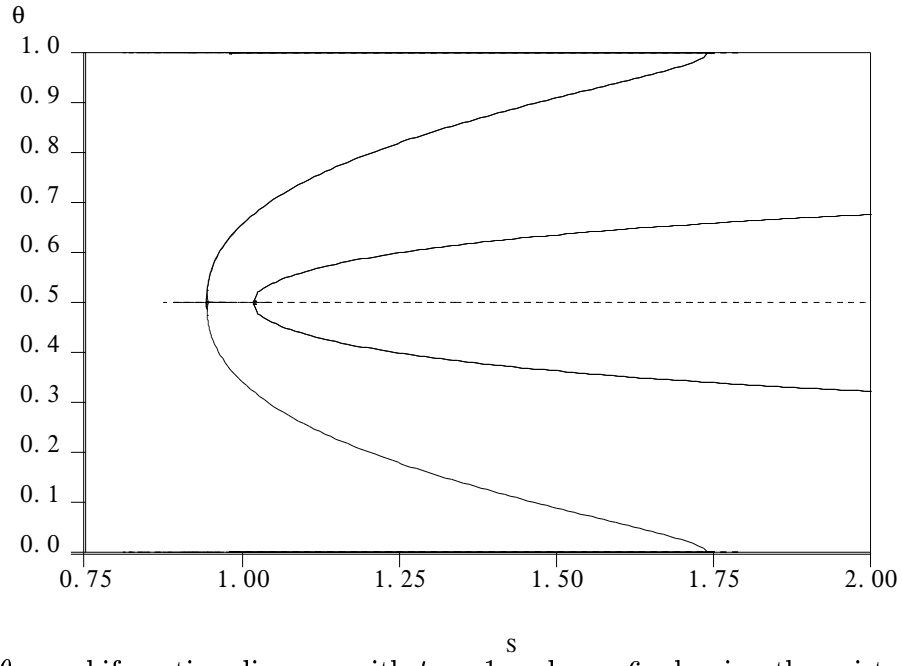

FIG. 9. θ vs s bifurcation diagram with $t_d = 1$ and $\alpha = 6$, showing the existence of multiple stable phase solutions for a given s, differing period (not shown) and phase of oscillation. Solid (dashed) lines indicate stable (unstable) solutions.

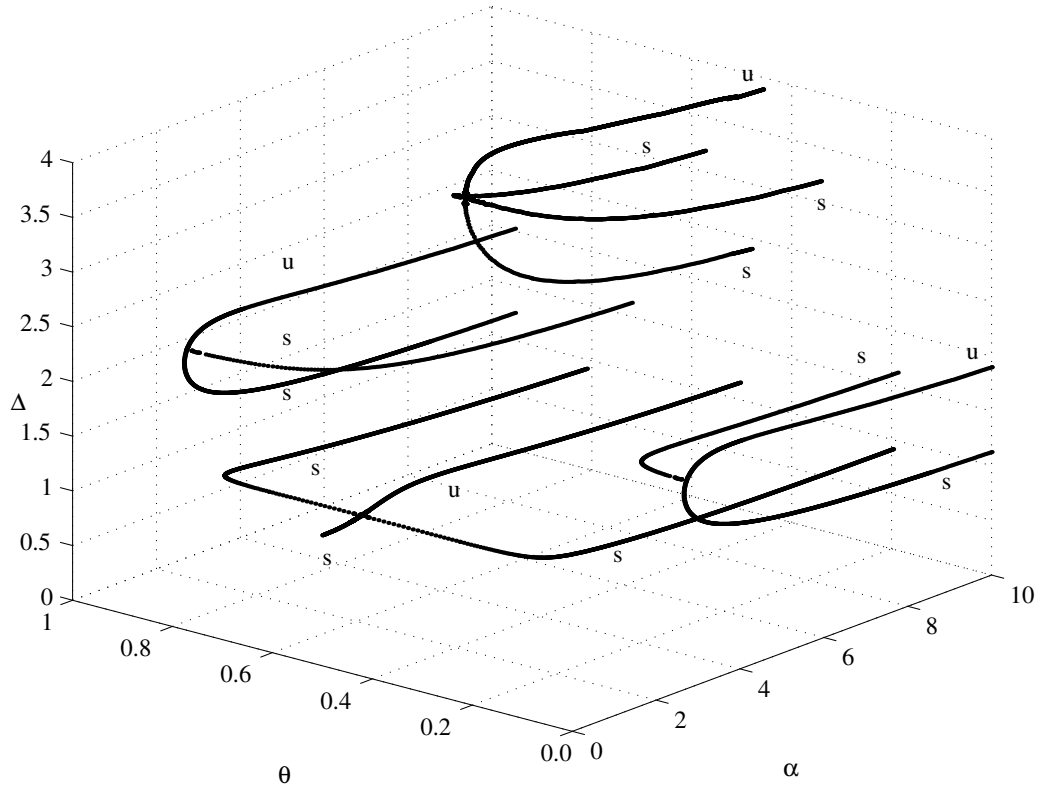

FIG. 10. θ vs α vs Δ bifurcation diagram with $t_d = 1$ and $s = 1.25$. The existence of multiple stable solutions is associated with the presence of a finite delay time t_d. s (u) labels stable (unstable) branches.

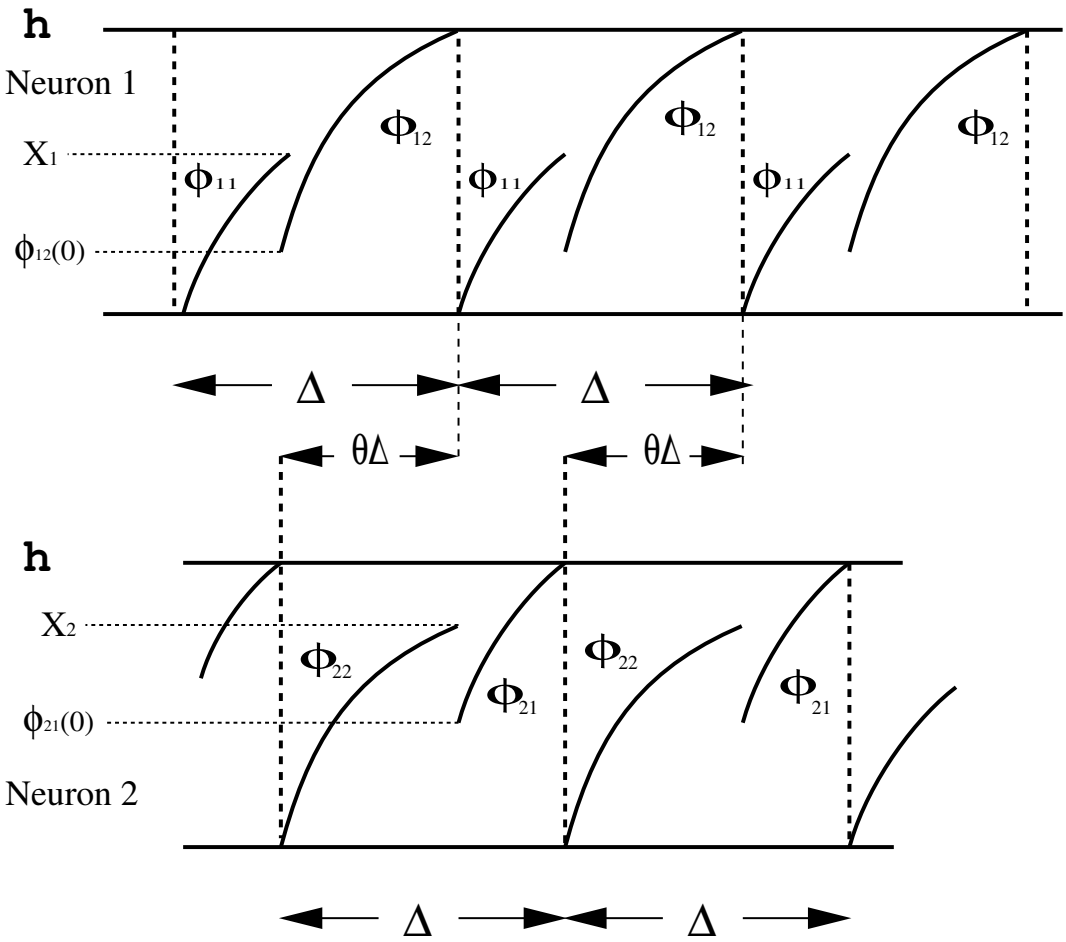

FIG. 11. Schematic diagram of the periodic solution for two pulse–coupled integrate–and–fire neurons with electrical coupling. The effect of reset is communicated between the two neurons via the direct electrical coupling and causes the discontinuous evolution of somatic potentials over a firing interval Δ.

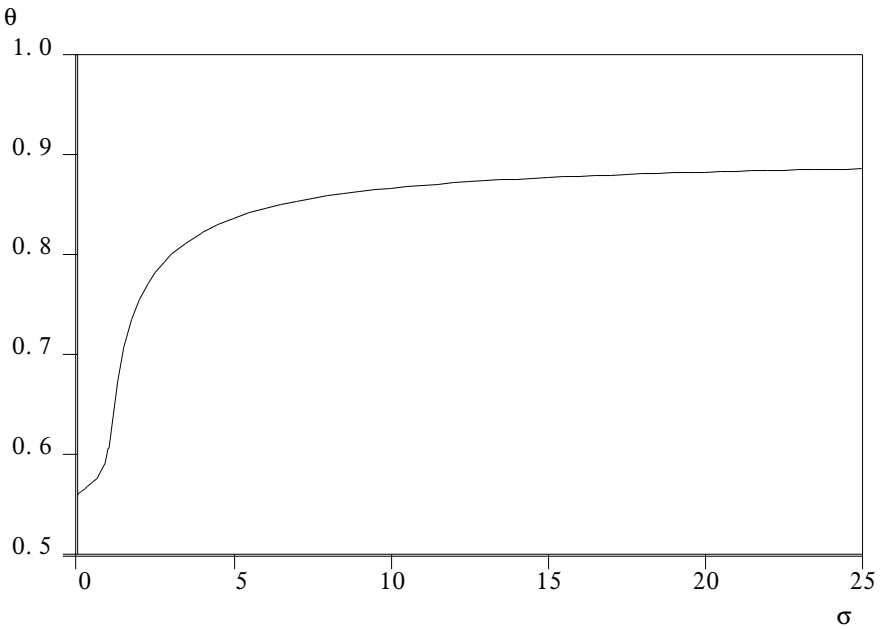

FIG. 12. Variation of phase θ in a network with both electrical and chemical coupling as a function of the strength of electrical interaction. $\alpha = 5.5$, $X_1 = 6.58 \times 10^{-2}$, $X_2 = 9.94 \times 10^{-2}$, $\phi_{12}(0) = 1.28 \times 10^{-3}$ and $\phi_{21}(0) = 4.08 \times 10^{-2}$.

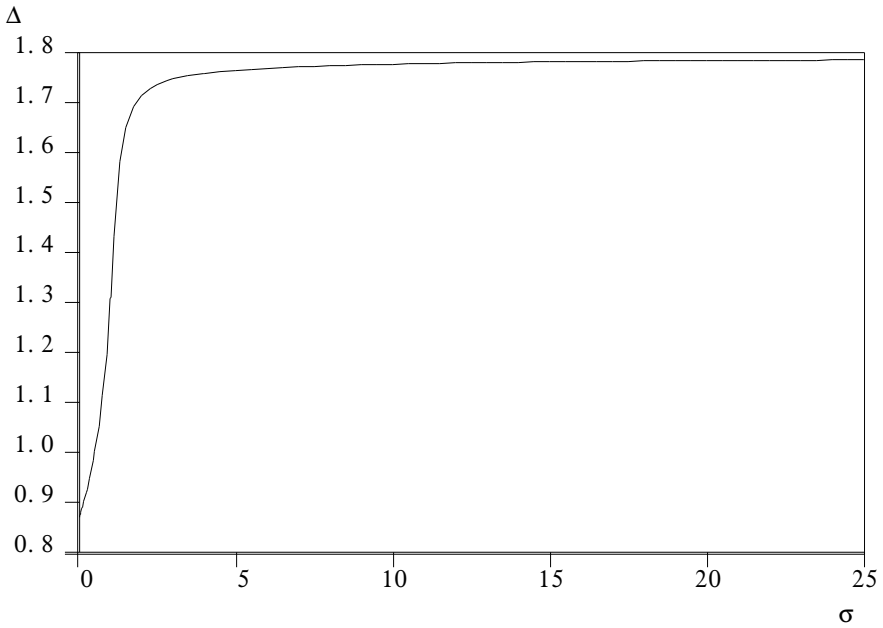

FIG. 13. Variation of period Δ for the system defined in figure 12, highlighting the functional significance of the strength of electrical interactin in modulating system firing frequency.

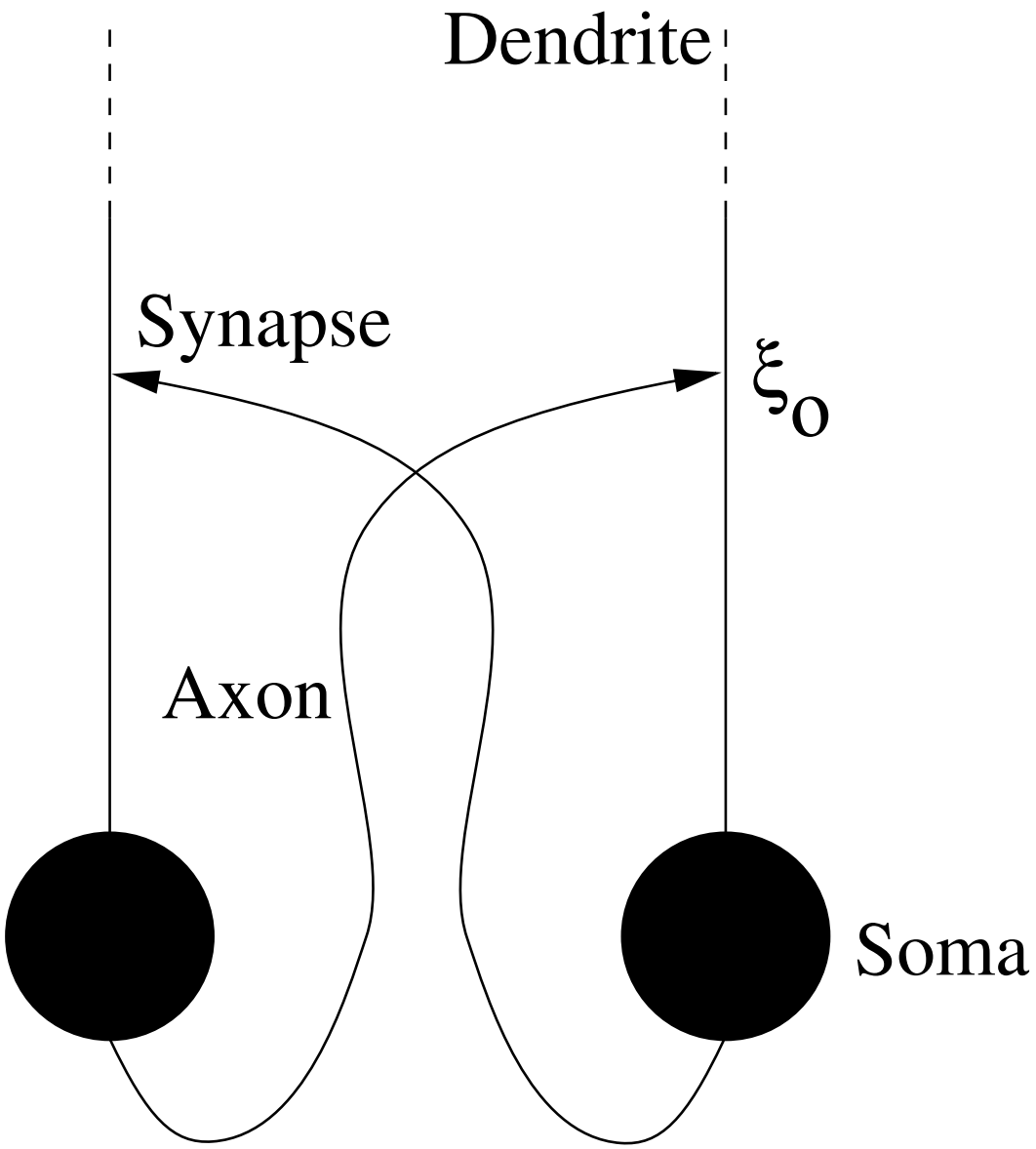

FIG. 14. Interaction schematic for two pulse–coupled integrate–and–fire neurons with idealised dendritic structure. Synaptic input occurs at synapses located a distance ξ_0 from the soma.

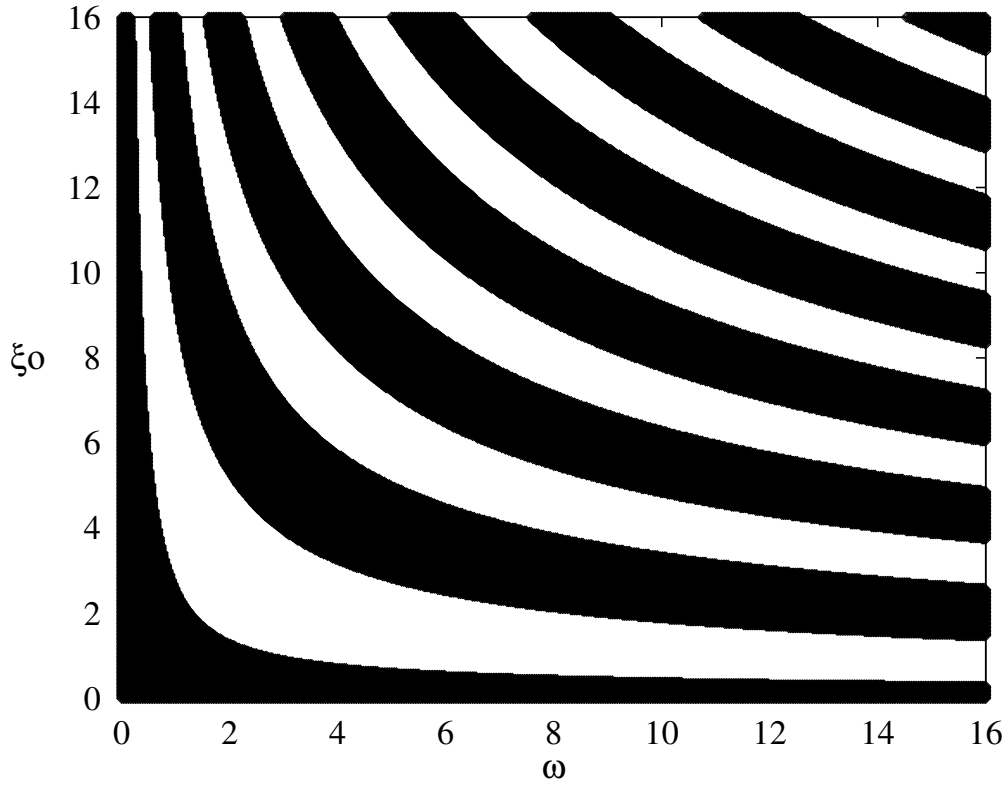

FIG. 15. Sign of $\widehat{A}$, ξ_0 vs ω. Black (white) regions correspond to $\widehat{A} > 0$ ($\widehat{A} < 0$). Note the checkerboard pattern of stability/instability, for say the synchronous solution, with increasing synaptic distance, ξ_0, for a fixed natural neuronal oscillator frequency ω.